Mixing in Ti/steel system under high-intense pulsed ion beam impact

N.N. Cherenda[a,b,*], V.I. Shymanski[a], A.Ya. Leyvi[b], V.V. Uglov[a,b], A.P. Yalovets[b], H.W. Zhong[c], S.J. Zhang[c], X.Y. Le[c], G.E. Remnev[d], S.Y. Dai[e,f]

[a] Belarusian State University, Minsk, 220030, Nezavisimosty ave., 4, Republic of Belarus

[b] South-Urals State University, Cheliabinsk, 454080, Lenina ave., 76, Russian Federation

[c] Beihang University, Beijing 100191, Xueyuan rd., 37, People's Republic of China

[d] Tomsk Polytechnic University, Tomsk, 634028, Lenina ave., 2, Russian Federation

[e] Key Laboratory of Materials Modification by Laser, Ion and Electron Beams (Ministry of Education), School of Physics, Dalian University of Technology, Dalian, 116024, Linggong rd., 2, People's Republic of China

[f] DUT-BSU Joint Institute, Dalian University of Technology, Dalian, 116024, Linggong rd., 2, People's Republic of China

Abstract

Structure, phase and element composition, surface morphology of Ti/steel system subjected to the treatment of high-intense pulsed ion beam were investigated in this work. Numerical simulation, scanning electron microscopy, energy dispersion X-ray microanalysis and X-ray diffraction analysis were used as investigation techniques. Ion beam impact with Ti/steel system was accompanied with surface layer ablation, melting, mixing and generation of shock waves. The findings showed that mixing efficiency was depended on the power of ion beam and number of pulses. The synthesis of the mixed layer with the thickness of ~ 2 μm containing FeTi and Fe_2Ti phases was observed just after one pulse of treatment with the energy absorbed by the surface layer of 3.1 J/cm^2. Ti concentration in the surface layer as well as intermetallides volume fraction was depended on the number of pulses. Growth of the pulse number led to more uniform distribution of Ti in the mixed layer. Synthesized surface layer possessed increased microhardness.

Key words:

High-intense pulsed ion beam, ion beam mixing, intermetallide, hydrogen storage, shock waves, ablation

---

Corresponding author: cherenda@bsu.by

Introduction

The intermetallic alloy FeTi has many interesting properties including high hardness and shape-memory effect (Benyelloul et.al., 2014). Besides that FeTi is a promising candidate as hydrogen storage material showing relatively good storage capacity of 1.9 wt.% (Benyelloul et.al., 2014; Checchetto et.al., 2003; Matsushita et.al., 2019; Nong et.al., 2014). At the same time crystalline FeTi experiences cracking on hydrogen absorption (Novakova et.al., 1998) thus amorphous materials or materials with nanocrystalline structure have greater practical potential. Formation of amorphous or nanostructured FeTi was reported by mechanical alloying of Fe-Ti powder (Adelfar et.al., 2019), magnetron sputtering (Balogh et.al., 1988) and arc melting with the following ball milling (Tajima et.al., 2013). Addition of alloying elements such as V and Cu can also be used for FeTi grains refinement (Kumar et.al., 2014; Zhou et.al., 2018).

Mixing of Fe/Ti layer(s) by ion beams can also be a promising technique for synthesis of FeTi surface layer with amorphous or nanocrystalline structure (Brenier et.al., 1987; Rajput et.al., 2008). In (Brenier et.al., 1987) formation of amorphous surface Fe_xTi_{100-x} alloys was found for composition range corresponding to $29 \leq x \leq 67$ by interaction of 800 keV Xe ions with Fe-Ti multilayered system. At the same time small thickness of FeTi layer (few hundreds of nm) is the main disadvantage of such an approach. The thickness of the mixed layer can be increased by the usage of high power particle beams. In (Cherenda et.al., 2008) it was shown that treatment of Ti/steel system by compression plasma flows (energy density absorbed by the surface layer ~ 13 J/cm^2 per pulse) resulted in the formation of the mixed layer with the thickness of ~ 10 μm. Change of the coating thickness from 0.5 μm to 5 μm led to the change of Ti concentration from 3 to 31 at.% in the mixed layer. As a result formation of Fe_2Ti compound was detected in the surface layer (for Ti coating thickness of 5 μm). Synthesis of the mixed layer under this type of treatment mainly occurs by convection whirls in the melt formed under the action of hydrodynamic instabilities at plasma-melt border (Cherenda et.al., 2017; Leyvi et.al., 2017; Cherenda et.al., 2019). The findings showed that concentration of Ti in the mixed layer was controlled mainly by the quantity of incorporated titanium (coating thickness) and thickness of the melt (energy absorbed by the surface layer). In order to increase Ti concentration up to ~ 50 at.% for this type of treatment it is necessary either to deposit Ti coating with greater thickness or to decrease energy absorbed by the surface layer. Increase of a coating thickness (deposited by cathodic arc vapour deposition) higher than a few μm can lead to it delamination from substrate. While the decrease of the energy lower

than the value of 10-12 J/cm^2 (by treatment with compression plasma flows) do not provide melting of Ti/Fe system surface layer and corresponding mixing in liquid state.

Another approach for FeTi surface layer synthesis by Ti/Fe system mixing is proposed in this work. It also includes cathodic arc vapour deposition of Ti coating with smaller thickness (0.5 μm) and following treatment by high-intense pulsed ion beam (HIPIB) that can produce melt layer with the thickness of the order of μm. Investigations carried out earlier showed efficiency of HIPIB mixing for Ni/Ti system (Yan et.al., 2007). Thus the synthesis of FeTi surface layer by HIPIB impact on Ti/steel system, investigation of synthesized surface layer structure and study of HIPIB treatment parameters influence on mixing efficiency were the aims of this work.

Experimental

The carbon steel polished samples of the following elemental composition: 0.2 C, 0.2 Si, 0.5 Mn (in weight percent) were used as substrates for coating deposition. The samples diameter was 14 mm and the thickness - 2 mm. The titanium coating was deposited on the samples by means of vacuum arc deposition with the following process parameters: the arc current of 100 A, the bias voltage of -120 V, the deposition time of 2 minutes. The pressure in the vacuum chamber during deposition was 10^{-3} Pa. The thickness of the coatings was 0.5 μm.

Steel samples coated with titanium were treated by HIPIB at BIPPAB-450 accelerator with a magnetic insulated diode at Beihang University (Zhang, et.al., 2015). The ion flux consisting of 70% H^+ and 30% C^{n+} was provided by using polyethylene anode. The pulse duration was 100 ns. Two different treatment regimes were used. At the first one the peak value of accelerating voltage was 450 kV, current density was 100 A/cm^2 and number of pulses was changed in the range of 1- 5. The corresponding energy density of heat flux absorbed by the sample (registered by calorimetric measurements) was 1.8 J/cm^2 per pulse. At the second regime the peak value of accelerating voltage was 390 kV, current density was 320 A/cm^2 and number of pulses was changed in the range of 1-15. The corresponding energy density absorbed by the sample was 3.1 J/cm^2 per pulse.

Numerical experiment on interaction of one pulse of high-intense pulsed ion beams with Ti/Fe system was carried out using software package BETAIN (Yalovets et.al., 2002). The system of equations (1)-(7) containing equations of continuum mechanics and wide-range equation of state was solved in one-dimensional Cartesian geometry using this package:

$$\frac{\dot{V}}{V} = \frac{\partial v}{\partial z}, \quad (1)$$

$$\rho \dot{v} = \frac{\partial \sigma_{zz}}{\partial z}, \quad (2)$$

$$\rho \frac{dU}{dt} = \sigma_{zz} \frac{\dot{V}}{V} + \frac{\partial}{\partial z}\left(\kappa \frac{\partial T}{\partial z}\right) + D(z,t), \quad (3)$$

$$\sigma_{zz} = -P(\rho,T) + S_{zz} + \delta\sigma, \quad (4)$$

$$P = P(\rho,T), \quad (5)$$

$$\dot{S}_{zz} = \frac{4}{3}\mu \frac{\partial v_z}{\partial z}, \ \dot{S}_{xx} = \dot{S}_{zz} = -\frac{2}{3}\mu \frac{\partial v_z}{\partial z} \quad (6)$$

$$S_{xx}^2 + S_{yy}^2 + S_{zz}^2 \leq \frac{2}{3} Y_0^2, \quad (7)$$

where V – volume, ρ – mass density; v – components of medium flow mass velocity; z – distance along the depth; t – time; U – internal energy; σ_{ik} – tensor of non-equilibrium stress; v_{ik} – tensor of deformation speed; κ – heat conductivity coefficient; T – temperature; δ_{ik} - Kronecker symbol; μ – shear modulus; D – energy release function; P – pressure that is determined by wide-range equation of state (5); S_{ik} - stress deviator. Equation (7) is the Mises yield condition, Y_0 is the yield stress. Nonequilibrium addition $\delta\sigma$ in equation (4) is caused by the rate of local change of the mass density of the medium during compression (Volkov et.al., 2010). Kinetic equation for fast particles (that is necessary to find energy release function) was added to the system of equations (1)-(7) (Val'chuk et.al., 1992).

The surface and cross-section morphology was analyzed with the help of scanning-electron microscopy (SEM) using the LEO 1455 VP microscope. The element composition analysis was carried out by energy dispersion X-ray microanalysis (EDX) using the Oxford X-ray detector. The surface layer phase composition was investigated by means of X-ray diffraction (XRD) with the Ultima IV RIGAKU diffractometer in Cu Kα radiation. The samples were weighed before and after HIPIB treatment by a RADWAG AS 60/220/C/2/N analytical balance with the mass determination accuracy of ± 0.05 mg. The microhardness was measured using the MVD 402 Wilson Instruments equipment (Vickers diamond indenter) at the load of 1.0 N.

Results and discussion

Numerical simulation

HIPIB interaction with material surface layer resulted in a number of effects influencing on it microstructure and properties including melting, ablation and stress generation (Le et.al., 2002; Zhang et.al., 2015). Thus numerical simulation of these physical processes was carried out for evaluation of HIPIB impact results on Ti/Fe system. At the first dependences of energy release in target along the depth for two treatment regimes were obtained using the beam

parameters and current-voltage characteristics (Figure 1). One can see main steps at these dependences corresponding to C^{++} and H^{+} projectile ranges. These dependences were used for further description of target substance thermodynamic parameters under high-intense pulsed ion beams impact.

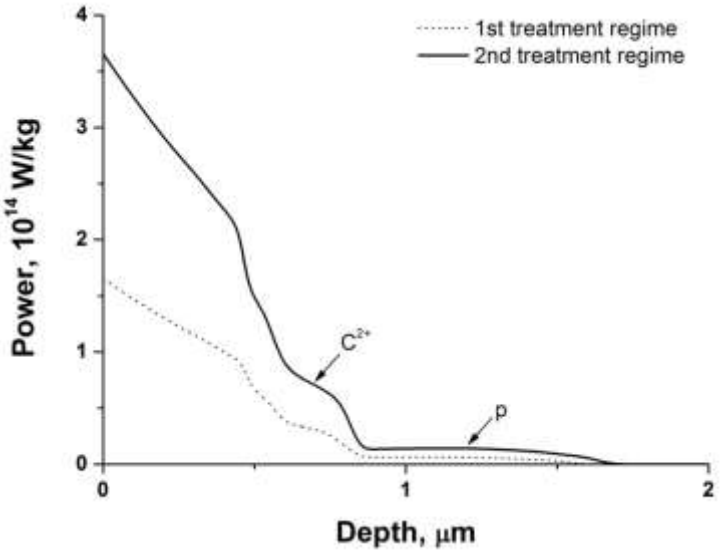

Figure 1. The dependence of energy release in target along the depth for two treatment regimes at 5 ns.

According to the results of numerical simulation HIPIB impact led to transition of Ti/Fe surface layer from solid to the liquid state and surface layer ablation. The speed of ablated target material spreading in direction opposite to movement direction of ion beam at the end of the pulse (100 ns) could reach up to $3 \cdot 10^5$ m/s for the first treatment regime and $7 \cdot 10^5$ m/s for the second one. Such a process could lead to diminishing of the Ti substance quantity that could take part in formation of the mixed layer (assuming insignificant redeposition of Ti atoms from the vacuum chamber after the end of the pulse). In particular relative density distribution ρ/ρ_0 (ρ – current density, ρ_0 –target density at normal conditions) along the depth of the target at two treatment regimes is shown at Figure 2. Depth coordinate 0 corresponds to initial target position (before ions impact). After the impact target started to expand and its free surface moved opposite to direction of ion beam, while the surface of target in condensed state moved in the direction of ion beam.

These simulation data showed that thickness of Ti coating diminished on 150 nm at the first treatment regime after one pulse. Increase of the beam power led to ablation of all Ti coating from Fe surface. At the same time no convection in the liquid state and Ti mass transfer into the depth of the target were taken into account during simulation.

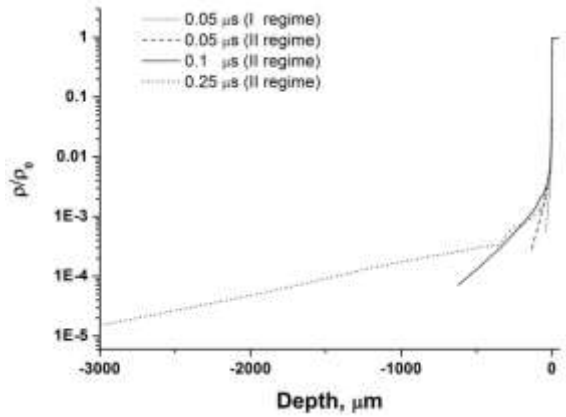

Figure 2. Target relative density distribution along the depth in different period of time.

Assuming that convection, in particular thermocapillary and concentrationcapillary convection (Volkov et.al., 2010), is the main mechanism of mass transfer in melted Ti/Fe system, then the thickness of the mixed layer will be approximately equal to the thickness of the melted layer. Thus the temperature distribution along the target depth was also determined for the estimation of the melted layer thickness (Figure 3 and 4). One can see that the temperature at the target surface could reach $7 \cdot 10^3$ K. The approximate thickness of the melted layer (determined on the melting temperature of Ti – 1943 K) in case of first treatment regime was about 2.5 μm while in case of the second treatment regime – 3.5 μm.

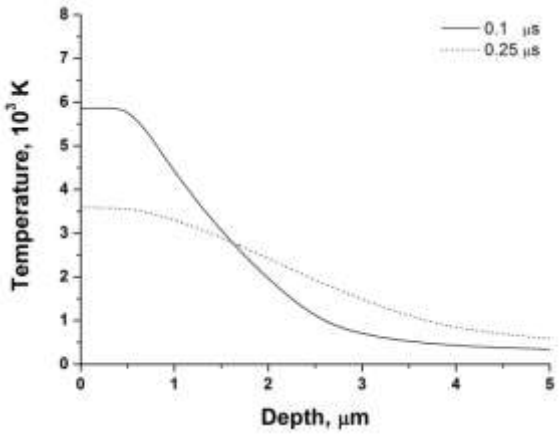

Figure 3. Temperature distribution along the target depth in case of the first treatment regime in different period of time.

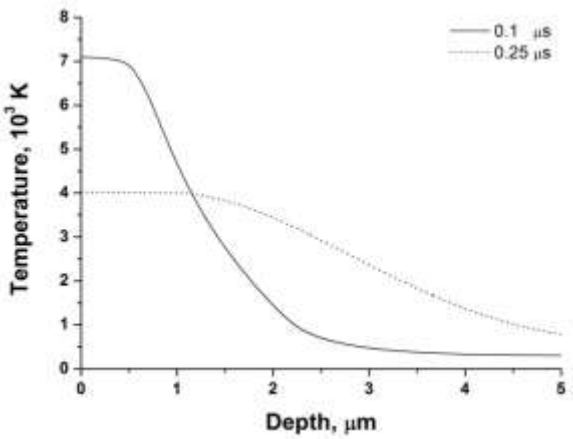

Figure 4. Temperature distribution along the target depth in case of the second treatment regime in different period of time.

Interaction of HIPIB with solids can lead to generation of the mechanical stress in the target (Dong et.al., 2007; Le et.al., 2002; Zhang et.al., 2019). The stress value can exceed yield strength of the material leading to cracks formation. There are two main mechanisms of stress

generation. First of them is connected with thermoelastic stress appeared due to the target layer heating (Zhang et.al., 2019). The thickness of the cracks containing layer is of the order of ions projectile range in this case. During impact of short-pulse particles beams stress can also appear due to surface ablation and formation of shock waves propagating into the target depth up to the back side of the sample with possible reflection from it (Dong et.al., 2007; Le et.al., 2002). In this case cracks can be found far beyond the target surface. The stress fields formed due surface ablation during HIPIB impact at two treatment regimes are shown at Figures 5 and 6. Shock wave possessed a complex form due to its distribution in different materials (Ti, Fe), different phases (solid, liquid) and reflection from material and phase boundaries. One can see that ion impact resulted in shock waves generation with the amplitude up to 1.25 kbar (125 MPa). This value is close to the yield strength of pure iron (170 MPa (Grigoriev, 1991)) and titanium (100 MPa (Grigoriev, 1991)). The amplitude of shock waves diminished during penetration deeper into the target.

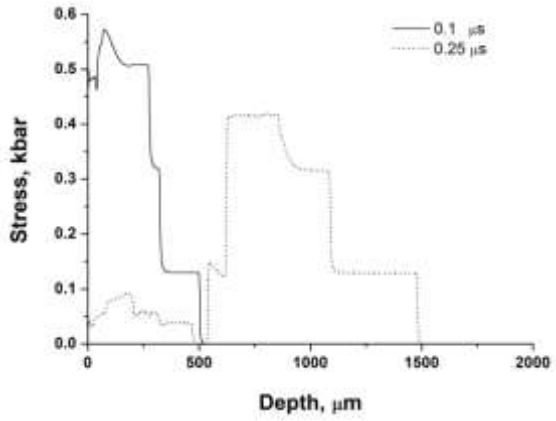

Figure 5. Stress distribution along the target depth in case of the first treatment regime in different period of time.

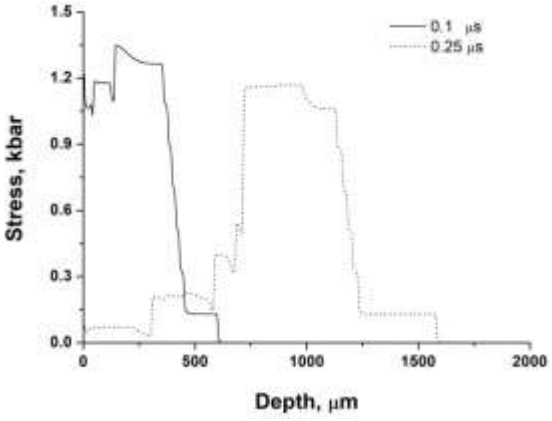

Figure 6. Stress distribution along the target depth in case of the first treatment regime in different period of time.

HIPIB treatment at 1.8 J/cm^2.

The influence of HIPIB treatment on the mixing efficiency can be roughly estimated using the data of SEM and EDX techniques. In the Figure 7 one can see surface morphology and distribution of elements along the line for the samples treated at 1.8 J/cm^2. Just after coating deposition the formation of Ti droplets on the surface was found (Fig. 7 a, b) that is characteristic feature of cathodic arc vapour deposition without filtering systems. HIPIB

impact led to the smoothening of the surface due to partial ablation of Ti droplets and surface layer melting. Besides that cracks formation was found at the surface (Fig. 7 c, e). Cracks appeared just after 1 pulse of treatment. Element contrast at SEM images formed by backscattered electrons and EDX data allowed concluding that iron atoms existed at the edge of some cracks on the surface (bright areas around cracks at Figs. 7 c, e). The findings also showed surface contamination by oxygen that was uniformly distributed along the surface.

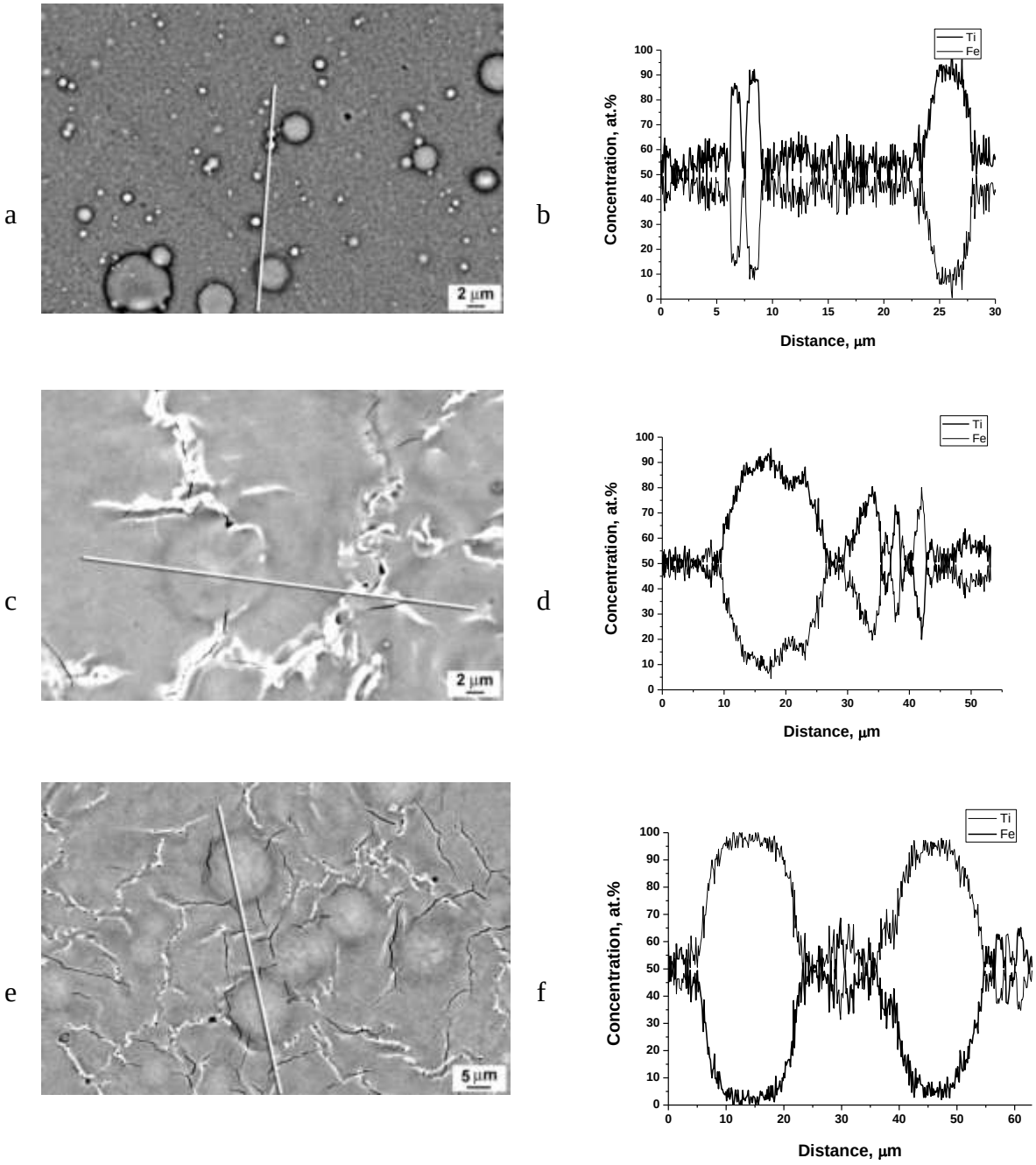

Figure 7. Surface morphology (a, c, e) and characteristic X-rays distribution of elements (b, d, f) in Ti coated steel sample (a, b) and Ti/steel samples after 1 (c, d) and 5 pulses (e, f) of HIPIB impact at 1.8 J/cm^2.

The data of cross-section morphology analysis of Ti coated steel sample (Fig. 8 a, b) showed that oxygen penetration into the growing Ti coating from the residual chamber could be one of the causes of oxygen presence in the surface layer. Though oxygen penetration also could take place from the residual atmosphere of vacuum chamber during HIPIB treatment. Cross-section analysis revealed that cracks existed only in the surface layer with the thickness comparable with the thickness of Ti coating (Fig. 8 c). That is why thermoelastic stress could be the main reason of cracks formation for this treatment regime.

HIPIB impact at 1.8 J/cm^2 did not lead to substantial mixing of Ti/steel system. At the same time formation of local mixing areas of different types between elements of substrate and coating can be seen on the cross-section of HIPIB treated samples indicating the beginning of mixing process (Fig 8 c, e). The first type of local mixing area is shown at Figure 8 c. This area contain crack with edges enriched with Fe atoms. Another type of local mixing area is shown at Figure 8 e. According to this figure preferential direction of mass transfer flow was perpendicular to the surface. The main reasons of these mixing areas appearance is the formation of local melting areas containing titanium coating and steel substrate as well as realization of conditions necessary for capillary convection or generation of hydrodynamic instabilities.

a 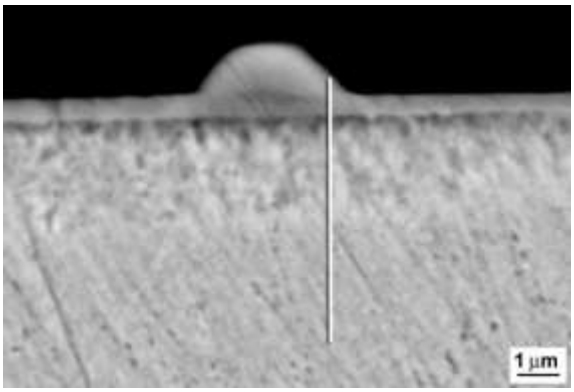

b 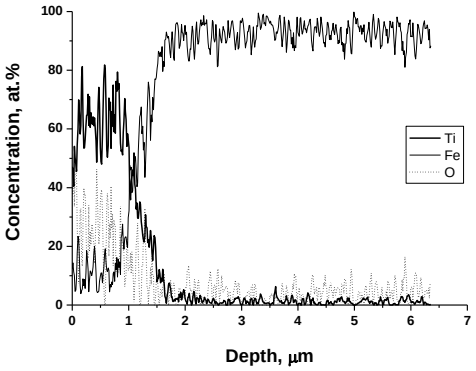

c 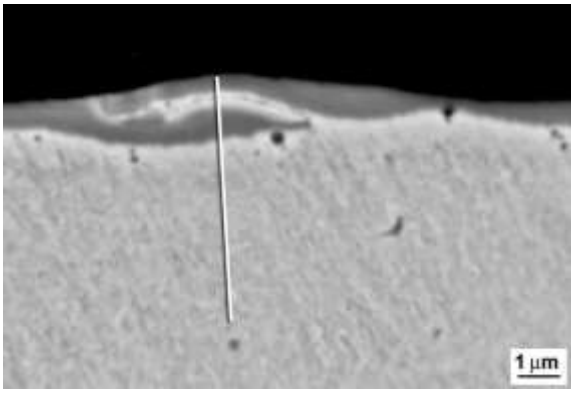

d 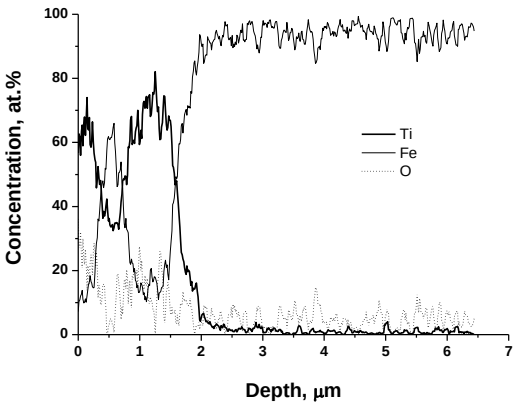

e

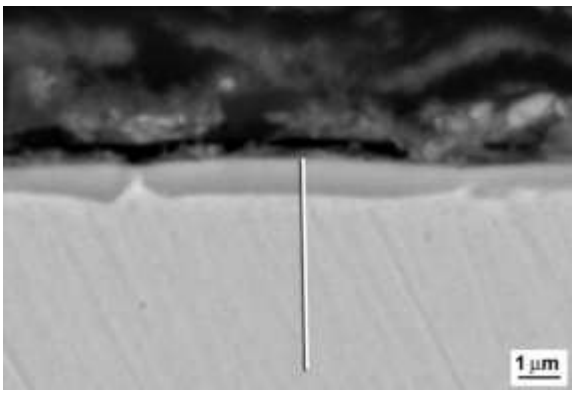

f

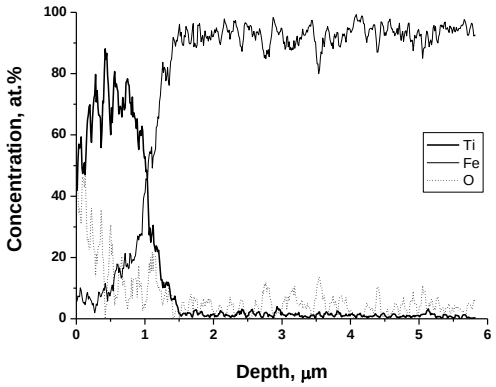

Fig. 8. Cross-section morphology (a, c, e) and characteristic X-rays distribution of elements (b, d, f) in Ti coated steel sample (a, b) and Ti/steel samples after 1 (c, d) and 5 pulses (e, f) of HIPIB impact at 1.8 J/cm^2.

The data of XRD analysis (Figure 9) showed that Ti diffraction peaks were still exist at the diffraction pattern of samples treated by HIPIB in accordance with the SEM data. At the same time the width of Ti diffraction peaks became larger that can be explained by the Ti grains refinement after crystallization of the surface layer melt or microstress increase in Ti lattice. TiO_2 (rutile) diffraction lines of low intensity were found at the diffraction patterns of all samples that is consistent with the data of EDX analysis. Only one new line (42.8 degrees) appeared at the diffraction patterns of the samples after treatment (Figure 9). This line can be interpreted as 100 % (110) FeTi diffraction line in spite of the fact that its angle position is slightly shifted to the area of lower diffraction angles being compared with the standard. Formation of intermetallic phase could take place in the areas of mixing between titanium coating and steel substrate (Fig. 8 c, e). Small intensity of FeTi diffraction lines as well as low mixing efficiency at this treatment regime did not allow determining dependence of phase transformation in the surface layer on the number of pulses.

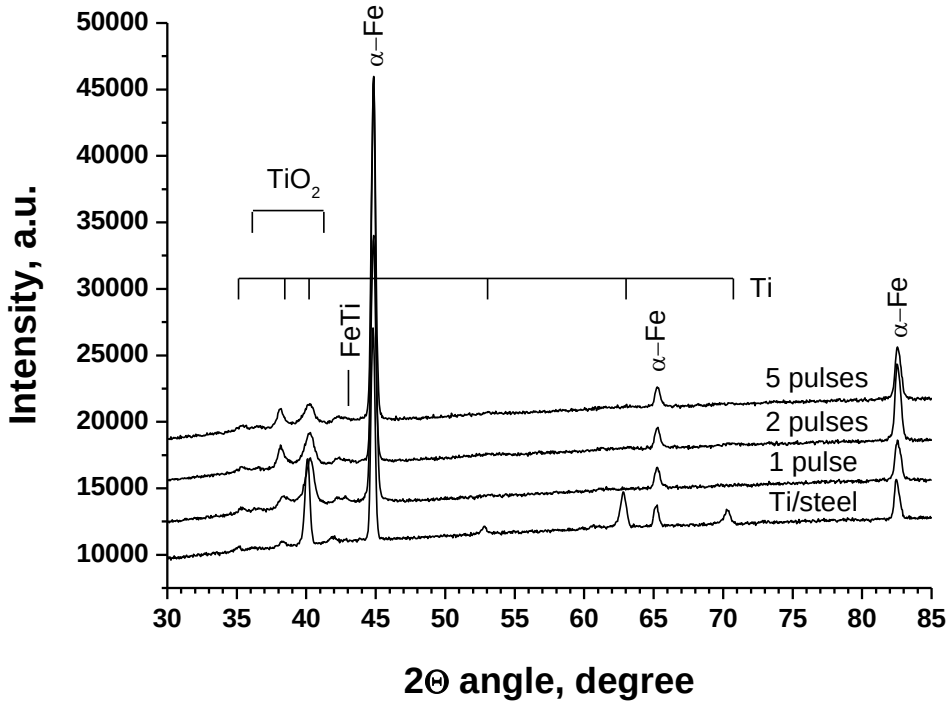

Figure 9. XRD patterns of Ti/steel system samples before and after HIPIB impact at 1.8 J/cm^2.

No microhardness changes of Ti/steel samples after HIPIB impact were revealed at this treatment regime.

HIPIB treatment at 3.1 J/cm^2.

In order to enhance mixing efficiency the power of ion beam as well the number of pulses were increased. Formation of the mixed layer was observed after 1 pulse of HIPIB impact. (Figure 10 a, b). The border between steel and mixed layer possessed wavy structure indicating formation of convective flows in the melt state. The border preserved it wavy shape with the increase of the pulse number though it became less expressed (Figures 10 c, d). After 15 pulses of HIPIB impact the mixed layer had relatively uniform structure. Its thickness was ~ 2 μm. This value correlated with the results of numerical simulation (~ 3.5 μm). It should be noted that during evaluation of the temperature fields in the surface layer ablation was not taken into account so the estimated value of the melt layer thickness was higher than experimentally determined.

Growth of the pulse number led to more uniform distribution of Ti in the mixed layer (Figure 10 b, d, e). The growth of mixing efficiency with the pulse number increase could be explained by the increase of convective flows duration that were responsible for mixing in the

melt. Besides that decrease of Ti concentration in the mixed layer was observed with the pulse number growth. Ti concentration of ~ 50 at. % was found after 1 pulse while after 15 pulses Ti concentration diminished up to 30 at. %. So HIPIB impact on Ti (0.5 μm)/steel system allowed to reach Ti concentration necessary to form FeTi compound by diminishing melt layer thickness in contrast to the results of work (Cherenda et.al., 2008). EDX analysis also revealed presence of oxygen in the mixed layer.

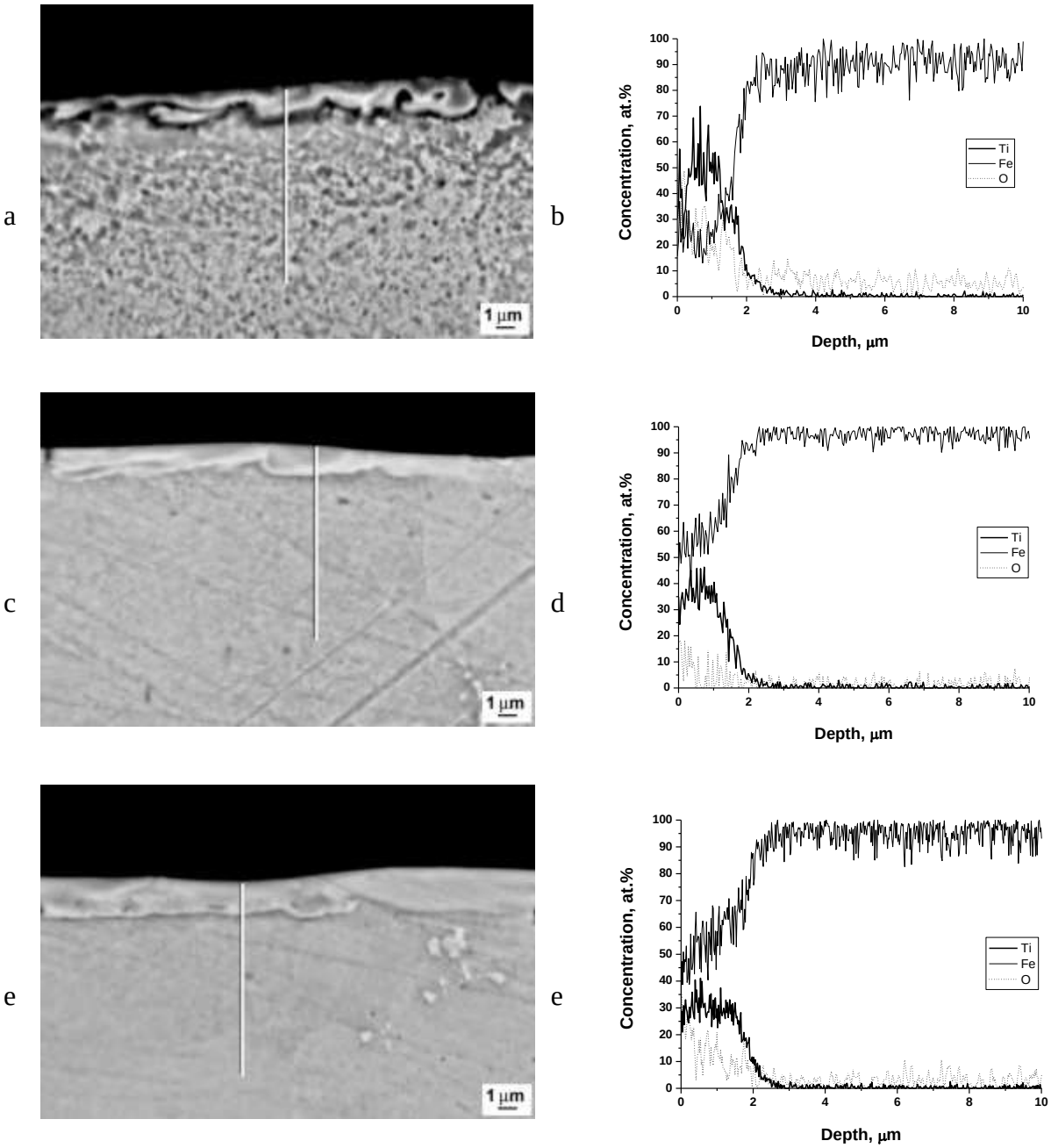

Figure 10. Cross-section morphology (a, c, e) and characteristic X-rays distribution of elements (b, d, f) in Ti/steel samples after 1 (a, b), 10 (c, d), and 15 pulses (e, f) of HIPIB impact at 3.1 J/cm^2.

HIPIB impact with Ti/steel samples at 3.1 J/cm^2 resulted in diminishing of the number of cracks at the surface (Figure 11) in contrast to the first treatment regime. Increase of structure homogeneity, more uniform elements distribution as well as increase of the melt quantity "curing" surface cracks appeared after the previous pulses could be the main reasons of this effect. The example of such "curing" is shown at Figure 11 a. In this case the length of crack was a few times greater than the thickness of the alloyed layer while in other cases cracks appeared in the mixed layer only (Figure 11 b). Besides that at the Figure 11 a one can see presence of cracks located far beyond the mixed layer. Similar effect was observed in Al after HIPIB treatment (Le et.al., 2002) and was explained by propagation of the shock waves into material depth. These results showed correlation with numerical simulation results for this treatment regime at which the generated stress value was close to the yield strength of Ti and Fe.

a) 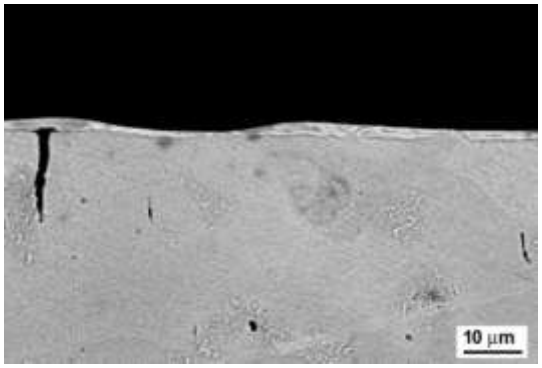

b) 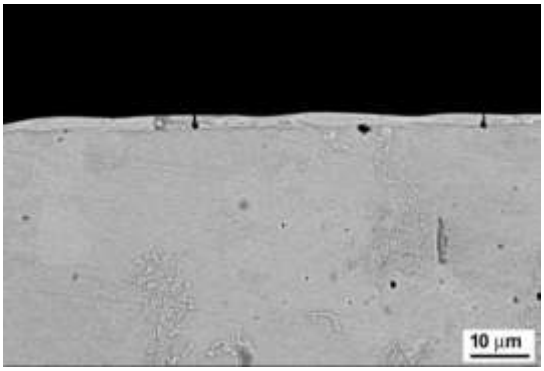

Figure 11. Cross-section morphology of Ti/steel samples after 10 (a) and 15 pulses (b) of HIPIB impact at 3.1 J/cm^2.

The decrease of Ti concentration in the mixed layer was connected with ablation of the surface layer. The results of numerical simulation were confirmed by experimental data (Figure 12). One can see that increase of the pulses number led to the growth of the mass deleted from the surface layer (except of the first pulse). Ablated material also contained Ti atoms that is why impact with each HIPIB pulse diminished quantity of Ti that can be redistributed in the melt layer by the next pulse. Deviation from the almost linear dependence of deleted mass on number of pulses at the one pulse treatment is explained by the presence of surface contamination after coating deposition. In particular if one normalize the deleted mass on the number of pulses, then after one pulse of treatment the maximum value of deleted mass per pulse is obtained, while the next pulses did not influence on the normalized value of deleted mass (Figure 12).

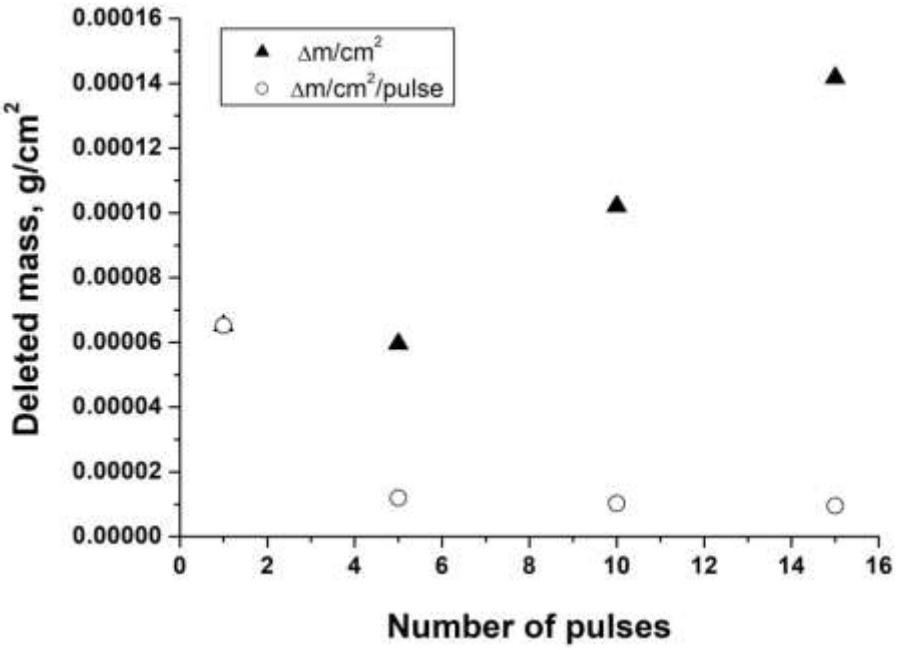

Figure 12. Weight loss of Ti/steel samples after HIPIB impact at 3.1 J/cm^2.

The data of phase composition analysis (Figure 13) corresponded to the data of cross-section morphology and element composition analysis. Increase of the pulses number from 1 to 5 led to disappearance of Ti diffraction lines. Besides that formation of FeTi and Fe_2Ti phases was found. Evaluation of FeTi grains (particles) size using the Sherrer's formula gave the value of a few tens of nm. The intensity of intermetallide phases diminished with the further growth of the pulses number (5 - 15 pulses) that was in agree with decrease of Ti concentration in the mixed layer. Ti concentration range of 30-50 at.% that was observed in the experiment corresponded at RT to the mixture of FeTi and Fe_2Ti phases according to the equilibrium Fe-Ti phase diagram (Adelfar et.al., 2019). Decrease of Ti concentration up to 30 at. % in equilibrium conditions should lead to the formation of Fe_2Ti only in the mixed layer. At the same time volume fraction of FeTi was much higher than volume fraction of Fe_2Ti that can be seen by the comparison of these phases diffraction lines intensity (Figure 13). That is why one may conclude the absence of Ti distribution homogeneity in the mixed layer and formation of local areas with different element concentration and phase composition. In this case presence of αFe(Ti) solution that also could give diffraction line at 2Θ=44.4 degree may be supposed. Increase of the pulses number also led to shift of FeTi diffraction line to the area of lower diffraction angle that could be connected with the deficiency of Ti atoms in FeTi crystalline lattice formed in conditions of high-cooling speed as well as with embedding of impurities into the crystalline lattice from the steel (C, Si, Mn) or vacuum chamber.

Presence of oxygen in the mixed layer resulted in TiO_2 formation as in the case of HIPIB impact at 1.8 J/cm^2.

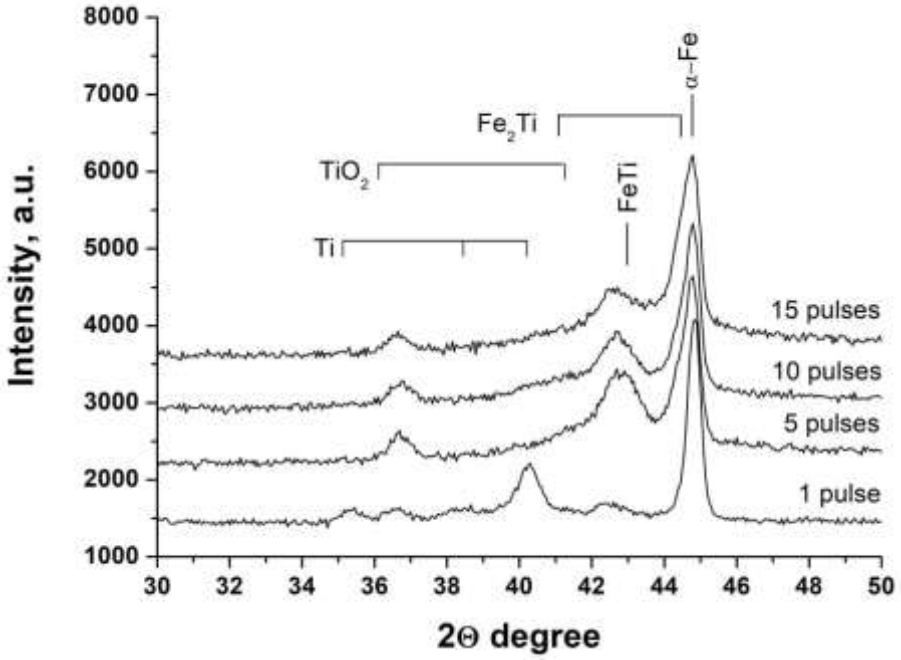

Figure 13. XRD patterns (glancing angle of incidence - 5^o) of Ti/steel system samples after HIPIB impact at 3.1 J/cm^2.

Microhardness measurements showed that number of pulses increase led to strengthening of the surface layer (Figure 14). Intermetallides formation should lead to the growth of surface layer microhardness. At the same time pulses number increase in the range of 5-15 pulses resulted in diminishing of FeTi volume fraction according to the XRD data. Thus monotonic microhardness increase could be explained by the increase of dislocation density due to shock waves propagation (Le et.al., 2002) or grains refinement in the mixed layer.

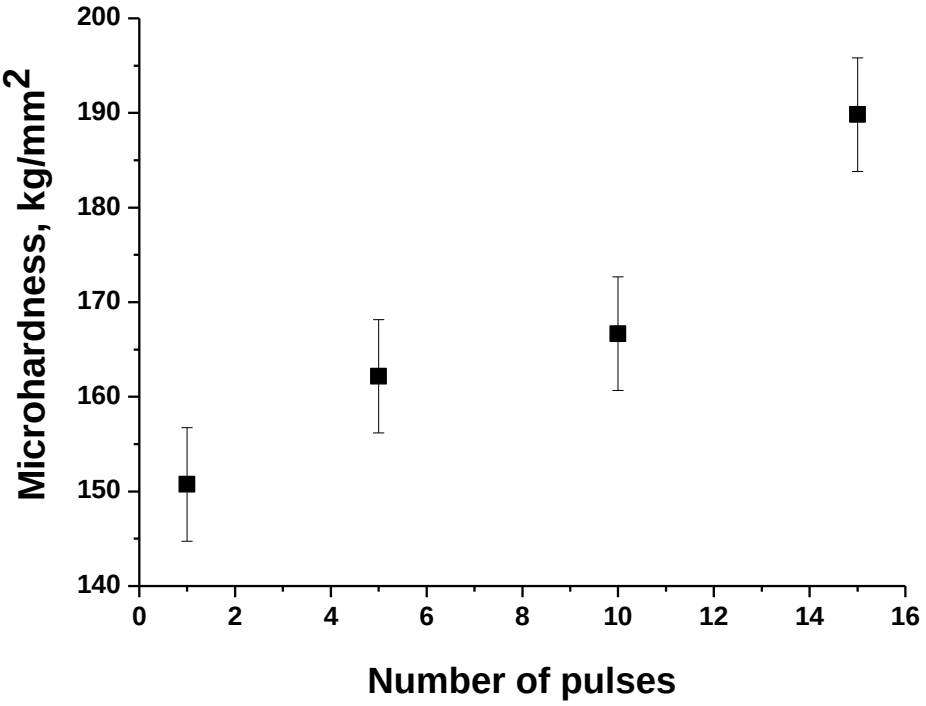

Figure 14. Microhardness of Ti/steel system samples after HIPIB impact at 3.1 J/cm^2.

Conclusions

An approach for FeTi surface layer synthesis consisting of cathodic arc vapour deposition of Ti coating on steel substrate and following treatment by high-intense pulsed ion beam (energy absorbed by the surface layer 1.8 and 3.1 J/cm^2/pulse) was proposed and realized in this work. According to the results of numerical simulation HIPIB impact led to transition of Ti/Fe surface layer from solid to the liquid state and surface layer ablation. The temperature at the target surface could reach $7 \cdot 10^3$ K. The approximate thickness of the melted layer in case of first treatment regime was about 2.5 μm while in case of the second treatment regime – 3.5 μm. Numerical simulation data showed generation of shock waves with the stress amplitude value close to the yield strength of pure iron and titanium. The results of simulation partially correlated with experimental data.

Experimental data showed that HIPIB impact at 1.8 J/cm^2/pulse (1-5 pulses) did not lead to substantial mixing of Ti/steel system. Formation of local mixing areas of different types between elements of substrate and coating containing FeTi phase were found. Thermoelastic stress appeared due to the heating of the surface layer was the reason of surface cracks formation.

Further increase of ion beam power (absorbed energy – 3.1 J/cm^2/pulse) resulted in the synthesis of the mixed layer with the thickness of ~ 2 μm just after 1 pulse of HIPIB impact.

Formation of surface cracks due to thermoelastic stress action and cracks in the bulk of the steel due to generation of shock waves was found. Growth of the pulse number led to more uniform distribution of Ti in the mixed layer. Besides that decrease of Ti concentration in the mixed layer from 50 at. % at 1 pulse treatment to 30 at. %. after 15 pulses was observed. The decrease of Ti concentration in the mixed layer was connected with ablation of the surface layer. The mixed layer contained FeTi and Fe_2Ti phases. The volume fraction of FeTi was much higher than that of Fe_2Ti and was depended on the number of pulses. Microhardness measurements showed that number of pulses increase led to strengthening of the surface layer.

References

Adelfar, R., Mirzadeh, H., Ataie, A., Malekan, M., Amorphization and mechano-crystallization of high-energy ball milled FeTi alloys, Journal of Non-Crystalline Solids, vol. **520**, p. 119466, 2019.

Balogh, J., Rodmacq, B., Chamberod, A., Metastable phase formation at the interface of compositionally modulated Fe-Ti films, Solid State Communications, vol. **66**, no 2, pp.143-147, 1988.

Benyelloul, K., Bouhadda, Y., Bououdina, M., Faraoun, H.I., Aourag, H., Seddik, L., The effect of hydrogen on the mechanical properties of FeTi for hydrogen storage applications, International journal of hydrogen energy, vol. **39**, pp. 12667 – 12675, 2014.

Brenier, R., Thevenard, P., Capra, T., Perez, A., Treilleux, M., Romana, L., Dupuy, J. and Brunel, M., Amorphous alloy formation by ion beam mixing of iron-titanium multilayers, Nuclear Instruments and Methods in Physics Research, vol. **B19/20**, pp. 691-695, 1987.

Checchetto, R., Bazzanella, N., Miotello, A., Principi, G., Deuterium thermal desorption from FeTi thin films, Journal of Alloys and Compounds, vol. **356–357**, pp. 521-525, 2003.

Cherenda, N. N., Uglov, V.V., Poluyanova, M.G., Astashynski, V.M., Kuzmitski, A.M., Pogrebnjak, A.D., Stritzker, B., The influence of the coating thickness on the phase and element composition of a "Ti coating / steel" system surface layer treated by a compression plasma flow, Plasma Processes and Polymers, vol. **6**, pp. S178-S182, 2009.

Cherenda, N.N., Malashevich, A.A., Uglov, V.V., Astashynski, V.M., Kuzmitski, A.M., The structure and phase composition of the U9 steel surface layer alloyed with chromium atoms under the action of compression plasma flow, J. Belarus. State Univ. Phys., vol. **2**, pp. 102–107, 2017. (in Russian).

Cherenda, N.N., Nichipor, V.Yu., Astashynski, V.M., Kuzmitski, A.M,. Oxidation resistance of steel surface layer alloyed by Mo and Cr under the action of compression plasma flows, High Temperature Material Processes, vol. **23**, no 3, pp. 209–219, 2019.

Dong, Z.H., Liu, C., Han, X.G., Lei, M.K., Induced stress wave on the materials surface irradiated by high-intensity pulsed ion beam, Surface & Coatings Technology, vol. **201** pp. 5054–5058, 2007.

Grigoriev, I.S. (Ed.), Phizicheskie velichiny: Spravochnik (Physical values: Handbook), Energoatomizdat, Moscow, 1991. (in Russian).

Kumar, S., Tiwari, G.P., Sonak, S., Jain, U., Krishnamurthy, N., High performance FeTi - 3.1 mass % V alloy for on board hydrogen storage solution, Energy, vol. **75**, pp. 520-524, 2014

Le, X.Y., Zhao, W.J., Yan, S., Han, B.X., Xiang, W., The thermodynamical process in metal surface due to the irradiation of intense pulsed ion beam, Surface and Coatings Technology, vol. **158 –159**, pp. 14–20, 2002.

Leyvi, A.Ya., Cherenda, N.N., Uglov, V.V., Yalovets, A.P., The impact of a shock-compressed layer on the mass transfer of target material during processing compression plasma flows, Resource-Efficient Technologies, vol. **3**, pp. 222–225, 2017.

Matsushita, M., Tajima, I., Abe, M., Tokuyama, H., Experimental study of porosity and effective thermal conductivity in packed bed of nanostructured FeTi for usage in hydrogen storage tanks, International journal of hydrogen energy, vol. **44**, pp. 23239 – 23248, 2019.

Nong, Z., Zhu, J., Yang, X., Cao, Y., Lai, Z., Liu, Y., First-principles study of hydrogen storage and diffusion in B2 FeTi alloy, Computational Materials Science, vol. **81**, pp. 517–523, 2014.

Novakova, A.A., Agladze, O.V., Sveshnikov, S.V., and Tarasov, B.P., Supersaturated solid solutions and metastable phases formation through different stages of mechanical alloying of FeTi, Nanostructured Materials, vol. **10**, no 3, pp. 365-374, 1998.

Rajput, P., Gupta A., Avasthi, D.K., Swift heavy ion induced modification in Fe/Ti system studied using X-ray waveguide structure, Nuclear Instruments and Methods in Physics Research, vol. **B266**, pp. 1680–1684, 2008.

Tajima, I., Abe, M., Uchida, H., Hattori, M., Miyamoto, Y., Haraki, T., Hydrogen sorption kinetics of FeTi alloy with nano-structured surface layers, Journal of Alloys and Compounds, vol. **580**, pp. S33–S35, 2013.

Val'chuk, V. V., Khalikov, S. V., Yalovets, A. P., Modeling the effect of intense charged particle fluxes on layered targets, Mathematical Modelling, vol. **4**, no 10, pp. 111-123, 1992. (in Russian).

Volkov, N. B., Leivi, A. Ya., Talala, K. A., Yalovets, A. P., Thermocapillary convection in a target irradiated by an intense charged particle beam, Tech. Phys., vol. **55**, pp. 484–490, 2010.

Yalovets, A.P., Mayer, A.E., Software package BETAIN (BEAM TARGET INTERACTION), Proceedings of the 6th Int. Conf. on Modification of Materials with Particle Beams and Plasma Flows, Tomsk, pp. 297-299, 2002.

Yan, S., Le, X.Y., Zhao, W.J., Shang, Y.J., Wang, Y., Xue, J., Study of metal film/substrate mixing by intense pulsed ion beam, Surface & Coatings Technology, vol. **201**, pp. 4817–4821, 2007.

Zhang, J., Yu, X., Zhong, H., Wei, B., Qu, M., Shen, J., Zhang, Y., Yan, S., Zhang, G., Zhang, X., Le, X., The ablation mass of metals by intense pulsed ion beam irradiation, Nucl. Inst. Methods Phys. Res., vol **B 365**, pp. 210–213, 2015.

Zhang, Q., Zhu, X.P., Zhang, C.C., Lei, M.K., Comprehensive material constraints incorporation in coupled thermalmechanical responses modelling for high-intensity pulsed ion beam processing of metals, Nuclear Inst. and Methods in Physics Research, vol. **B 461**, pp. 283–291, 2019.

Zhou, S., Xu, Y., Liao, B., Sun, Y., Dai, X., Pan, H., In-situ synthesis of Ti-Fe-based alloys prepared by the combination of mechanical alloying and laser melting deposition: Microstructure and corrosion resistance, Journal of Alloys and Compounds, vol. **768**, no 5, pp. 697-706, 2018.